Full paper

Synthesis and Characterization of Doped and Undoped Nano-Columnar DLC Coating

Foo Jin Hoe[a*], Tatsuhiko Aizawa[b], Satoru Yukawa[b]

[a]*Fakulti Kejuruteraan Mekanikal, Universiti Teknologi Malaysia, 81310 UTM Johor Bahru, Johor, Malaysia*
[b]*Department of Engineering & Design, Shibaura Institute of Technology*

*Corresponding author: jinhoe@fkm.utm.my

Graphical abstract
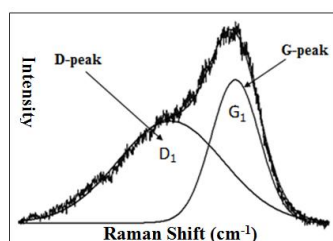

Abstract

Amorphous carbon (a-C:H/a-C) or Diamond-like carbon (DLC), has a very high potential diverse engineering and medical application for high wear resistance and tribological performance. Naturally grown columnar DLC films were chemically modified by post-treatment via electron beam irradiation (EB-irradiation). Precise observation and characterization is carried out by field emission scanning electron microscopy (FE-SEM), atomic force microscopy (AFM), and Raman spectroscopy. This nano-columnar a-C:H film has a unique nano-structure and mechanical properties which composed of graphitic inter-columnar network with amorphous carbon columns. Metallic doping into the inter-columns reflects positively on mechanical response by chemical modification with physical hardening.

Keywords: Nano-columnar DLC; EB-irradiation; FE-SEM; AFM; Raman spectroscopy; doping

Abstrak

Karbon amorfus (a-C:H/a-C) ataupun Diamond-like karbon, mempunyai pelbagai potensi kejuruteraan yang sangat tinggi serta applikasi perubatan untuk rintangan haus yang tinggi dan prestasi tribologi. Kolumnar DLC filem adalah diubahsuai dengan pos-rawatan melalui alur elektron penyinaran (EB-irradiation), pemerhatian yang tepat dan terperinci kemudian dilakukan melalui field emission scanning electron microscopy (FE-SEM), atomic force microscopy (AFM), dan spektroskopi Raman. Nano-kolumnar filem a-C:H ini mempunyai nano-struktur dan sifat-sifat mekanikal yang unik. Struktur nano-kolumnar ini terdiri daripada rangkaian graphitic antara kolumnar dengan lajur karbon amorfus. Doping logam ke dalam ruang antara kolumn memberi gambaran positif melalui pengubahsuaian kimia dalam respons mekanikal dengan pengerasan fizikal.

Kata kunci: Nano-kolumnar DLC; EB-irradiation; FE-SEM; AFM; spektroskopi Raman; doping

■1.0 INTRODUCTION

Over decades, sputtering techniques was the dominant method for film deposition from the carbon targets with the use of gases like argon mixed with reactive component like H_2, N_2 and/or hydrocarbons. Diamond like carbon (DLC) coating has mechanical properties fall between those of graphite and diamond. Various kinds of DLC coating have been developed over the years to have different mechanical and electrical properties depending on the type of deposition methods.[1] It has the significant potential to improve the surface properties, by high hardness, low wear rate, low friction coefficient, excellent tribological properties and good corrosion resistance. DLC is also an excellent candidate to be used as biocompatible coatings on biomedical implants.

Properties of amorphous carbon films deposition depend much on the processing parameters during the film deposition. Most of recent researches on the carbon-based materials pay more attention to nano-structured system and its applications. However, most of the commercial available DLC films with/without doping have no intrinsic characteristic of nano-structure

One of the authors found out that physical vapor deposition (PVD) oriented amorphous carbon films should have nano-columnar structure on the substrate by the means of chemical modification via EB-irradiation process.[2] Precise characterization were carried out by Raman spectroscopy and AFM on the nano-columnar DLC films formation.[3] On the other hand, the in-plain correlation factor (La) is estimated through Raman Spectroscopy peak observation; the integrated peak intensity ratio of I(D)/I(G) to describe the binding state and also estimate the nano-structure size.[4] Therefore, it provides valuable information regarding the growth parameters that allow uniform growth of nano-columnar DLC films.[5] In the present paper, self-organization on nano-columnar DLC is described and considered by using RF-sputtering in addition to EB-irradiation process. Their precise observation, evaluation and characterization on the nano-columnar DLC are very important.

2.0 NANO-COLUMNAR AMORPHOUS CARBON COATING DESIGN

2.1 Nucleation and Growth Mechanism

In general, the nucleation and growth mechanism of amorphous carbon films is classified by two extremes; i.e. three dimensional (3D) growth from nucleates and two dimensional (2D) growth via homogenizing by activated species in deposition.[6] Stranski-Krastanov growth as schematically illustrated in Figure 1 is an intermediary process, which is characterized by both 2D layer and 3D island formation after nucleation. The 3D columnar structure formed in the film had a characteristic and vague column-to-column separation[7]; its low density inter-columnar region has sometimes many voids as also illustrated in Figure 1.[8]
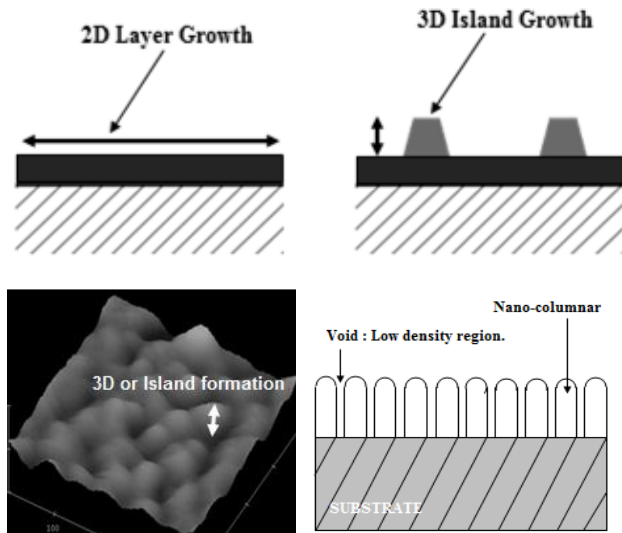

Figure 1 Stranski–Krastanov growth (Nano-columnar DLC)

　　In the case of PVD coating, the above growing mechanism is shown in Figure 2, empirically summarized as the Thornton structure model. Considering that PVD takes place under pressure ranging from 0.1 Pa to 3 Pa and at low temperature, amorphous carbon is expected to grow in rough columnar manner within T1 range (Zone 2).[9]

2.2 Weak Beam and Solid Interaction

EB-irradiation is an effective process to control the phase and microstructure via solid-beam interaction. High dose or high energy irradiation leads to severe structural modifications at the surface in the bulk[10]; e.g. beam induced transformation from crystalline to amorphous. On the other hand, the low energy electron in the order of keV penetrates and interacts only with the top surface with no means to deteriorate the chemical and physical characteristics of the substrate materials.[11] This weak solid-beam interaction suggests that the film once deposited, should be modified chemically as a post-treatment to tailor a desirable microstructure.[12] Low energy electrons generate less heat; in fact, maximum temperature rise is still limited by 200 K.[13] Low energy electrons were applied to rearrange the structure during the interface.[14]
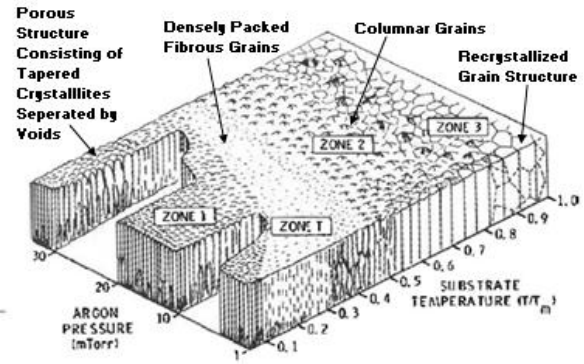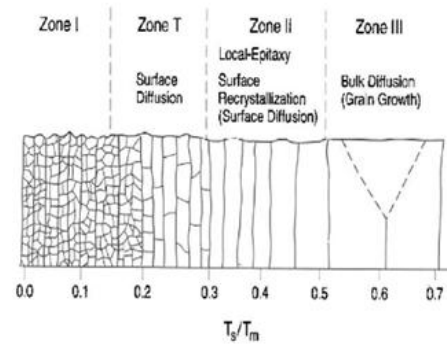

Figure 2 Thornton structure model

3.0 EXPERIMENTAL PROCEDURE

3.1 Preparation of DLC Film

Either doped or undoped, DLC films with the thickness of 400 nm were deposited on silicone substrates with the use of tailor-made RF-sputtering machine (Shinko Seiki Inc.; SRV6201) with 13.56 MHz. The sputtering pressure and substrate temperature were selected to make amorphous carbon grow in the three dimensional structure. Figure 3 shows and illustrates the present RF-sputtering system with vacuum chamber, matching box, control-units and chiller.
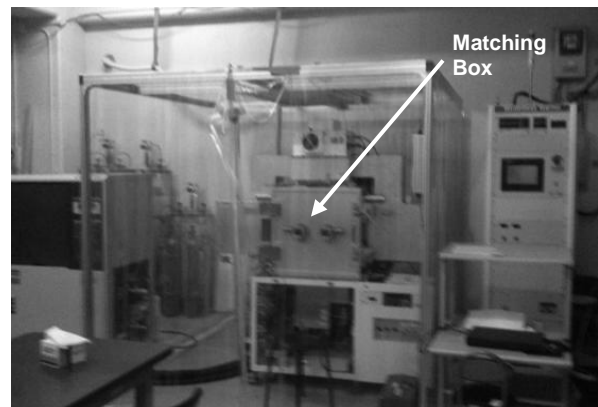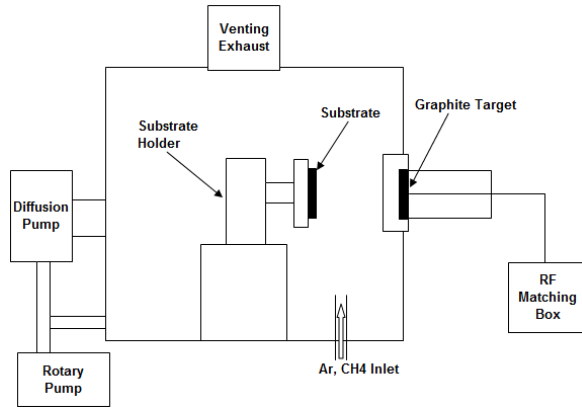
Figure 3 RF-Sputtering system for DLC coating

In this PVD approach, DC-bias as well as substrate temperature, are independently controlled. Carbon plume generated from graphite target reacts with a carrier gas of argon-diluted methane in the plasmas. Reactants are deposited onto a substrate to form a-C:H film. This coating process is tuned up by RF-power, DC-bias, target-substrate distance and substrate temperature, respectively. In addition, total carrier gas pressure and gaseous components have significant influence on this physical process. Silicon substrate of size $10 \times 10 \times 0.5$ mm^3 is used for microstructure analysis and observation. Among these various parameters is shown in Table 1, those parameters are fixed except for pressure.

Table 1 Experimental condition in RF sputtering

RF-Power	**700 W**
Target-Substrate Distance	**150 mm**
Base Pressure	**5×10^{-4} pa**
Ar:CH$_4$ Ratio	**90:10**
Bias Voltage (DC-bias)	**0 V**
Pressure	**0.5, 1.0, 1.5, 2.0 Pa**

In the metallic doped DLC films, it exhibit several enhanced properties which includes superior tribological properties. In the doping process, copper foil was glued onto the carbon target so that Cu could grow with carbon in the matrix.

3.2 Electron Beam Irradiation

The Mini-EB (Ushio, Inc.) system for low energy EB-irradiation is deployed as illustrated in Figure 4. It consists of EB tube, EB housing, and a high voltage power supply. This EB-irradiation is with a dose rate of $6.0 \times 10^{11} s^{-1} mm^{-2}$. The DLC film were homogeneously irradiated with an electron beam in a vacuum chamber with a selective electrical potential and irradiation current as shown in Table 2. In order to prevent oxidation, the substrates were kept under a nitrogen atmosphere. The flow rate of the nitrogen gas was around $10.0 Ls^{-1}$.

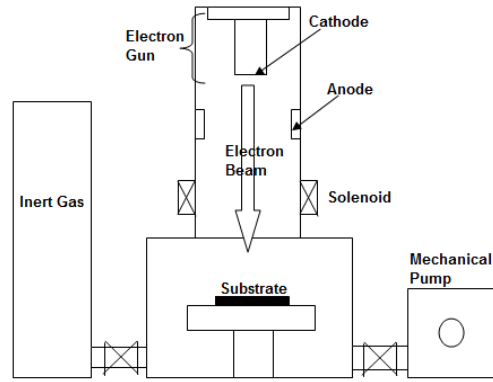**Figure 4** Schematic diagram of mini-EB

Table 2 Experimental condition in EB-irradiation

Dose Rate	**6.0×10^{11} S^{-1} mm^{-2}**
Accelerated Voltage (V$_A$)	**60 kV, 30 kV**
Current (I$_A$)	**300 mA, 150 mA**
Time Duration	**1000 s, 3000 s**

3.3 Raman Spectroscopy

Raman spectroscopy is a technique widely utilized the structural content of the deposited films and also measures the ratio of sp^3 and sp^2 bonded states in the DLC films. Each characteristic vibration mode related to each carbon bonding stage is detected and analyzed to describe each contribution of carbon bonding. Raman spectroscopy (Jasco NRS-2100) was used for characterization of the amorphous and ordered states in a-C:H films.

3.3.1 Profile Analysis

This measured spectrum of a-C:H is fitted into G and D peaks with Gaussian function, as in Figure 5. The amorphous carbon initially has two broad peaks, i.e. the G- peak (around 1600 cm^{-1}, graphitic peak corresponding to sp^2, planar carbon bonding state) and D- peak (around 1320 cm^{-1}, diamond peak corresponding to sp^3, tetragonal carbon bonding state). The profile located in the lower wave number represents D-peak, corresponding to sp^3, the other, in the longer wave number, G-peak, corresponding to sp^2.
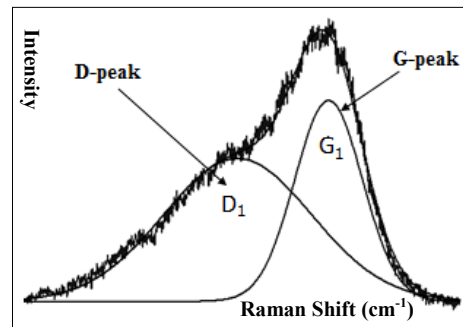

Figure 5 Typical chemical shifting in Raman spectroscopy

3.3.2 Area Intensity Ratio

Intensity ratio is often used for characterization of DLC films, for example, the increment of I(D)/I(G) ratio means an increase in the number/or the size of sp^2 in the matrix.[15] The intensity ratio, I(D)/I(G) is proportional to the in-plain correlation length, La.

3.3.3 Evaluation of Ordered States

Tuinstra and Koenig states that the relative intensity ratio of the D- and G- peak is inversely proportional to the in-plane correlation length (La) by Raman spectroscopy,[16] as shown in Figure 6. The correlation length may correspond to the actual columnar size. Disorder and weak localization is invoked to account for the broadening in the amorphous carbon. I(D)/I(G) is proportional to the number of rings at the edge of the grain and this relationship cannot be zero La.
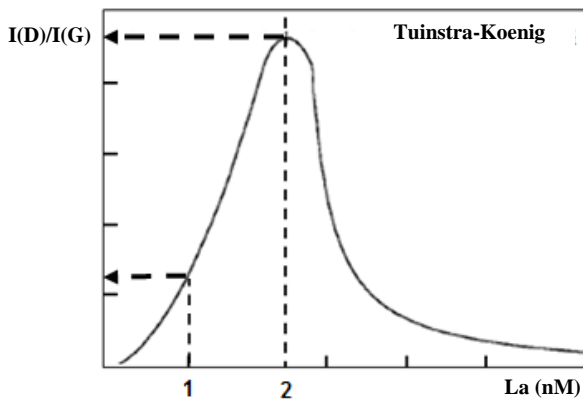
Figure 6 Variation of Raman I(D)/I(G) peak intensity ratio with in-plain correlation length (La). The Tuinstra-Koenig relationship

These nano-columns will continue to broaden along the y-axis with a constant growth until it touches the neighbor along the axis, that is, the direction perpendicular to the deposition plane. This nano-columns size increase as the growth time increases, and, as a result of that, well-aligned nano-columns can be formed.

3.4 Atomic Force Microscopy

AFM is one of the leading tools for imaging, measures at nano-scale. AFM generally can be operated for possible imaging mode in static (or, contact) mode and dynamic (or, non-contact) mode depending on the application and expectation required by user. During the measurement/observation, the measuring of the tip-to-substrate distance (x,y) data point allows the software to construct a topographical imaging for the substrate surface, hence, the DLC film can be examined for the elastic distribution with nanometer spatial resolution by using AFM. It would response to the inclination during measurement and it increases with the surface stiffness. Thus, the elastic distribution imaging for the DLC film and also the topographical image can be observed simultaneously.[17]

AFM is deployed to allow real time visualization of the dynamic interface.[18] Combination of AFM and other method such as SEM and Raman spectroscopy has been proposed for the characterization of DLC films.

3.5 Field Emission Scaning Electron Microscopy

FESEM scan the substrate with high energy beam of electrons in a rectangular shaped scanning pattern. The electrons will interact with the atoms and produced signals that contain information about the substrate's surface topography, and properties. Due to the narrow shaped scanning electron beam pattern, the SEM micrographs have a large depth of field yielding a characteristic 3D appearance which is useful for in order to understand the surface structure of the substrate. A wide range of magnifications is possible for microstructure surface or cross-sectional observation.

3.6 Nano-Indentation

Nano-indentation is a powerful technique for studying and proving film's mechanical properties such as hardness (H) and Young's modulus (E) on a nanometer scales. With hardness is being defined as the maximum indentation load divided by the projected contact area and the Young's modulus determined from the slope (dP/dh) of the unloading load-displacement curves.

During measurement, various parameters such as the load and depth of penetration were recorded and the load-displacement curve can be plotted to determine the mechanical properties of the material. The average Young's modulus (E) and hardness (H) are obtained from this measurement. The sharp indenters causes the yielding of the indented material at a lower load and thus also permit one to access the properties of very thin films. dP/dh, the slope of curve in Figure 7, upon unloading in indicative of the stiffness of contact. This indicates the response of material tested and the device itself.
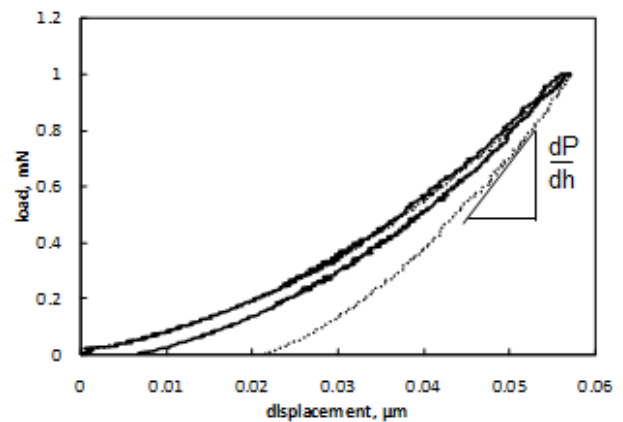
**Figure 7** Schematic of load-displacement curve

■4.0 RESULTS

4.1 Characterization of Carbon Films

Characterization of amorphous carbon is most commonly done by determining the ratio of sp^2 (graphite) to sp^3 (diamond) hybridized bond in the deposited films. This sp^2 to sp^3 ratio is defined by counting the number of carbon atoms in planar bonding versus those in tetragonal bonding in local micro-structure.

The thickness of the DLC films is determined using the SEM cross-sectional views in Figure 8(A). It is controlled to be 400nm for all substrates, with a deposition rate of 3.4nm per minute. On the other hand, Figure 8(B) shows the cross-sectional view of Cu-doped DLC film after EB-irradiation, with a measured thickness

of around 400 nm as well. In the undoped film, distinguished contrast like shown in Figure 8(B) is not observed. Copper is, in nature, has a larger atomic mass than carbon. Hence, the shinny white region corresponds to the presence of Cu. Other than that, bright spots is observed on the columnar structure, which implies the segregation of copper taken place in the inter-columnar region due to copper's little affinity with carbon.[4]
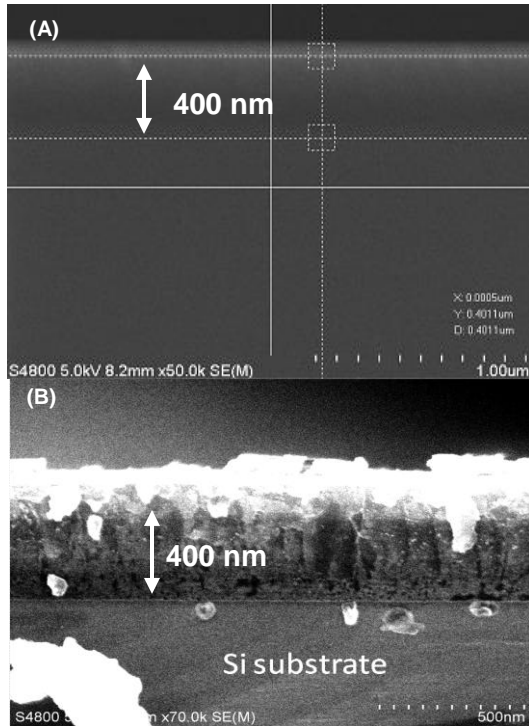

Figure 8   Cross-sectional view of FE-SEM images of DLCfilms (A) Undoped, (B) Cu-doped

After EB-irradiation, the nano-columnar size is larger than that in the as-deposited film; e.g. 1.5 nm (as-deposited film), 7.1 nm at 1000 s in EB-irradiation and 14.4 nm at 3000 s as shown in Figure 9. In Figure 10, it clearly shown the growth in size for the individual nano-columns occurs as the EB-irradiation time increases.[19] The columnar diameter (D) is associated with film thickness due to low thermal stability and shadowing effect of the film structure.
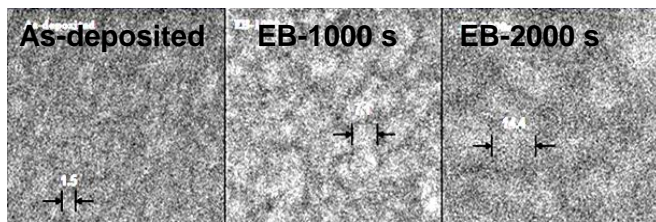
Figure 9   Planar view of FE-SEM images of DLC films
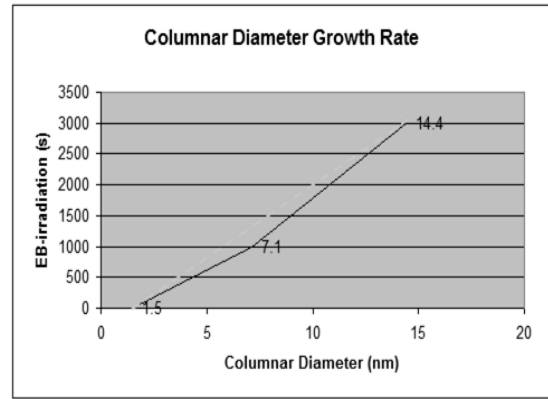
**Figure 10**   Columnar diameter growth rate
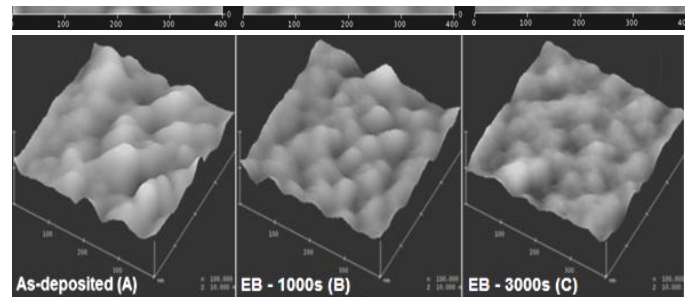
Figure 11   The AFM images and the topological profile image (A), (B), and (C)

Figure 11 shows some typical AFM images of the film deposited. In the 2D and 3D imaging for the DLC film measured by the AFM, it is easily noticed that before EB-irradiation, this DLC films was seen in the image as vague, random and naturally grown columnar structure. The amorphous to columnar structure is modified by EB-irradiation and this chemically modified film has a fine nano-columnar structure where low-density columns are surrounded by high-density inter-columnar regions. Inter-columnar regions have low density sometime with voids, which is where the amorphous carbon starts to make ordering.

After EB-irradiation, the surface appears to be smoother, void-free and more homogeneously distributed. The original vague nano-structure is modified to be more organized nano-columnar through self-alignment, i.e. ordering taken place with increase EB time.

Figure 12 (A) and (B) shows the evolution of surface topographies for doped/undoped DLC films, with very obvious improved differences can be observed in the doped DLC.
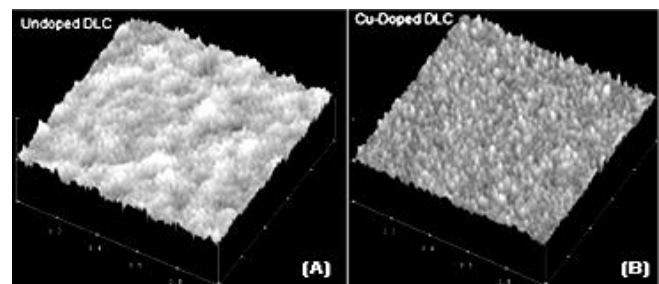
Figure 12   Topological profile image for undoped (A) and doped (B) substrate

Raman effect is used to analyze the structure of the RF-deposited DLC films, the positions of D- and G- peaks would shift upwards and the I(D)/I(G) ratio would rises. This suggests that the clustering (L_a < 2nm) of sp^2 into an ordered rings. Also, the increasing in I(D)/I(G) and the up-shifting in the G-peak are associated with a decrease in the sp^3 content. In another words, graphitization of C had taken place. The width of a peak, closely related to a distribution of clusters with different orders and sizes, appear to be on a rise with increasing RF power.
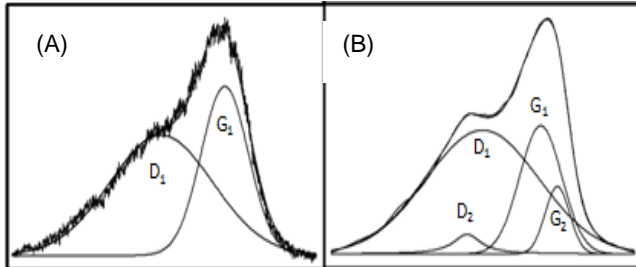
Figure 14 Comparison of the measured Raman Spectrum: (A) As-deposited, (B) After EB-irradiation

The Raman spectrum of DLC coating before EB-irradiation has two broad peaks (Figure 14(A)), i.e. the G-peak corresponding to graphitic peak of higher wave number of C-C bonding, and the D-peak, to disorder-induced peak at its lower wave number. A clear D-peak appears in the as-deposited substrates and then with the gradual sp^2 clusters growth causes the G-peak to gradually increase in the subsequence substrates. This is shown by the monotonic increase of I(D)/I(G).

Figure 14(A) shows the as-deposited substrate, with D-peak of 1400 cm^{-1}, G-peak of 1600 cm^{-1} and with I(D)/I(G) of 1.58. The in-plain correlation length (La), estimated at La = 1 nm. The initial films have amorphous state with no ordered structure in it. Figure 14(B) shows the spectra for EB-irradiated substrate. Note that there are no significant changes of D- and G- peak for both spectra in Figure 14 (A) and (B).

The EB-irradiated substrate were characterized by 4 peak profiles, where the emerging of new D_2 and G_2 peaks, corresponding to the initial amorphous matrix, D_1 and G_1, i.e. the as-deposited DLC film. Their calculated correlation length: La, is estimated around 2 nm for $I(D_1)/I(G_1)$ of 2.56. As mentioned above, the new D_2 and G_2 peaks appear in Figure 14(B), showing a great different in term of their bonding state after EB-irradiation. $I(D_2)/I(G_2)$ is 0.46. The detail comparison of the D- and G- peak intensity by Raman spectroscopy is shown in Table 3.

Table 3 Comparison of the D- and G- peak intensity by Raman spectroscopy

	Centre	FWHM	I(D)/I(G)
As-deposited			
D_1	1400.0 cm^{-1}	370.0 cm^{-1}	1.58
G_1	1600.0 cm^{-1}	117.0 cm^{-1}	
	Centre	FWHM	I(D)/I(G)
After EB			
D_1	1396.6 cm^{-1}	356.1 cm^{-1}	2.56
G_1	1552.5 cm^{-1}	133.0 cm^{-1}	
D_2	1355.0 cm^{-1}	90 cm^{-1}	0.46
G_2	1597.1 cm^{-1}	133.0 cm^{-1}	

Figure 15 shows the Raman spectra for Cu-doped substrate, with D-peak of 1390 cm^{-1}, G-peak of 1560 cm^{-1} and I(D)/I(G) is 1.59. The in-plain correlation length (La), estimated at La = 1 nm. The initial films have amorphous state with no ordered structure, and it also showing no changes even with Cu-doped in it. Figure 15(B) shows the EB-irradiated undoped and Cu-doped substrate respectively. Also, note that there are no significant changes of D- and G- peak for both spectra in Figure 15 (A) and (B).

Similar to the undoped substrate, this Cu-doped substrate is also characterized by 4 peak profiles, with the emerging of new D_2 and G_2 peaks. Their calculated correlation length: La, is estimated around 2 nm for $I(D_1)/I(G_1)$ of 2.11. As mentioned above, the new D_2 and G_2 peaks appear in Figure 15(B), showing a great different in term of their bonding state after EB-irradiation. $I(D_2)/I(G_2)$ is 0.30 respectively. The detail comparison is shown in Table 4.
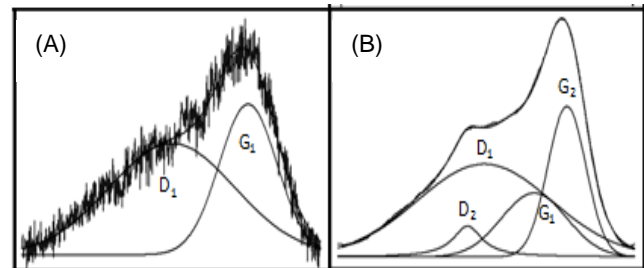
Figure 15 Comparison of the measured Raman Spectrum: (A) Cu-doped as-deposited, (B) Cu-doped after EB

Table 4 Comparison of the D- and G- peak intensity by Raman spectroscopy

	Centre	FWHM	I(D)/I(G)
As-deposited			
D_1	1390.0 cm^{-1}	360.0 cm^{-1}	1.59
G_1	1560.0 cm^{-1}	123.0 cm^{-1}	
	Centre	FWHM	I(D)/I(G)
After EB			
D_1	1382.5 cm^{-1}	397.7 cm^{-1}	2.11
G_1	1508.0 cm^{-1}	193.7 cm^{-1}	
D_2	1340.0 cm^{-1}	90 cm^{-1}	0.3
G_2	1590.1 cm^{-1}	112.8 cm^{-1}	

Either in the films, with or without doping, the newly generated phase of EB-irradiated film shows an apparently more graphitized state from the ratio of its integrated peak intensity with the in-plain correlation length estimated to be 14.5 nm (without doping) and 14.6 nm (with cu-doped), which is nearly the same with the average diameter of columns measured in the planer view of SEM image, i.e., 14.4 nm. Again, this implies that graphitization is accompanied with nano-columnar ordering.

4.2 Mechanical Properties of DLC Films

The mechanical properties of DLC films are very important in their application especially as protective coating. Figure 16 shows the comparison of doped/undoped load-unloading curve of a DLC films. The hardness (H) is defined as the pressure under the tip, given by the ratio of the force to the projected plastically deformed area (h_p). A tangent is drawn to the unloading curve at maximum load and the extrapolated to zero loads. The Young's modulus is proportional to the slope of this tangent line. The plastic deformation is h_p and the elastic deformation is the length from the intercept h_p to the maximum indentation h_{max}.
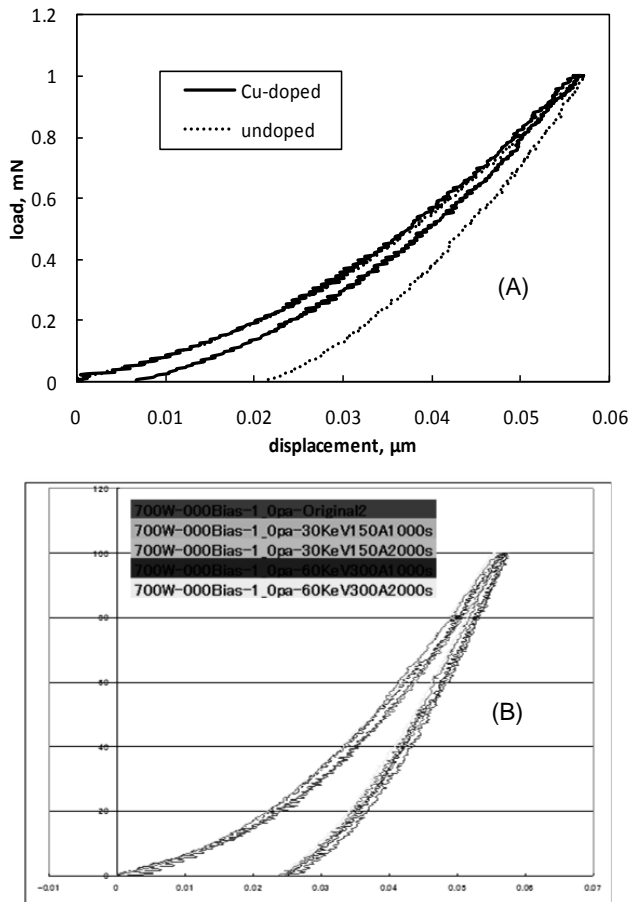
Figure 16 Comparison of the load-displacement curve, (A) doped/undoped, (B) EB-irradiated

Indentation load was set at a constant of 0.98 mN. The indentation depth ratio is set and controlled to be around 1/6 of total film thickness to eliminate the possibilities of substrate effect during the indentation measurement. Larger hysteresis between loading-unloading curves is observed for the as-deposited DLC film. Very little or no changes is observed in the linear elasticity in the loading process. However, there is a remarkable differences is obtained in the unloading curve, whereas the Cu-doped substrate shows a great elastic recovery characteristic comparing to the as-deposited substrate and it is reversible up to 12% of the film thickness. The dP/dh, slope of curve upon unloading is indicating of the stiffness S of contact.

Table 5 Comparison of the mechanical properties of DLC films measured by nano-indentation

	Hardness	Young's Modulus
Undoped as-deposited	1150	2.34×10^4
Undoped after-EB	1071	2.11×10^4
Cu-doped after-EB	1166	2.26×10^4

Hence, indicating $E_{Cu-doped} > E_{Undoped}$ as shown in Table 5, stating the value of 2.26×10^4 and 2.11×10^4, also, the $H_{Cu-doped} > H_{Undoped}$ of 1166 and 1071 respectively. As summarized in Table 5, Cu-doped film clearly has a larger hardness value over the undoped as-deposited and undoped after EB substrate even thou it has a more graphitized structure.

■5.0 DISCUSSION

Owing to precise observation, analysis and characterization, enough evidence shows that the modification of nano-structures occur with related to EB-irradiation time (in seconds), ordering take place and under the observation of FESEM (Figure 9), gradual increment of nano-columnar diameters from 1.5 (as-deposited) to 7.1 (EB-irradiation time 1000s) and 14.4 (EB-irradiation time 3000s) nm. Similarly, from Figure 11, the same conclusion can be made from AFM that the vague nano-structures are modified from the observed uneven structure to a gradually flatter structure.

Raman spectroscopy is frequently employed for the characterization of ordered state in amorphous carbon. The solid curves are Lorentzian curve fittings, no significant peak shift is observed for both D- and G- peak. From the ratio of the integrated peak intensity, let it be undoped or Cu-doped, the newly generated phase of EB-irradiated film has an apparently much more graphitized state. Also noted that the in-plain correlation length is estimated to be 14.6 nm, and, this almost coincides with the average columns diameter measured from the planer view of FE-SEM image.

The ordering process should have significant role in the exotic behavior of this modified nano-structure. Larger hysteresis between loading and unloading curve is observed and it is noted that it has a non-linear elasticity pattern. Little or no change in the linear elasticity is seen in the loading process. However, the most remarkable difference is seen in the subsequence unloading curves. This behavior is clearly due to the nano-columnar structure induced by EB-irradiation, the Cu-doped substrate showing the greatest elastic recovery as compared to the as-deposited and undoped substrate, with reversible up to 12% of the film thickness.

Moreover, as shown in Table 5, the Cu-doped film has a higher hardness even though it has a more graphitized structure. This Cu-doped nano-structure is embedded with plenty of Cu in the disordered state amorphous carbon matrix. This enhancement in hardness is due to the higher stiffness and ductility of Cu as compared to graphite. The presence of Cu in the inter-column, is reflects on softening, induced by chemically modifying and physical hardening.

■6.0 CONCLUSION

Summarizing, the DLC thin films with or without dopants were successfully produced on silicon. It is then chemically modified so to have fine nano-columnar structure via low-dose EB-irradiation. The nano-sized columnar network of graphitized inter-columns is embedded in the amorphous carbon matrix. This nano-columnar DLC film had high hardness and Young's modulus, in particular, has nonlinear elasticity so that 8 to 10 % of thickness becomes reversible under loading.

Our results confirm that with dopant incorporated into the DLC films, and due to copper-doping into the inter-columnar region, the above mechanical properties and performance of nano-columnar DLC coating are more improved toward applications.

Acknowledgement

References

(1) M. Sedlacek, B. Podgomik, J. Vizintin. 2004. *Material Characterization*. 59: 151.
(2) T. Aizawa, E. Iwamura, T. Uematsu. 2008. *Journal of Material Science.* 43: 6159.
(3) J. Foo, T. Aizawa, T. Uematsu. 2011. 5th SEATUC Symposium. PP 433.
(4) Y. Satoru, T. Aizawa. 2011. J-Global. 23: 6.
(5) J. Foo, T. Aizawa, T. Uematsu. 2012. 6th SEATUC Symposium. PP 143.
(6) A. Baskaran, P. Smereka. 2011. *Journal of Applied Physics*. 111: 111.
(7) T. Karabacak, G. C. Wang, T. M. Lu, 2004. *J. Vac. Sci. Technol*. 22: 1778.
(8) S. H. Woo, Y. J. Park, C. K. Hwangbo. 2006. *AJSTD*. 24: 153.
(9) J. M. Lacknew, W. Waldhauser, A. Alamanou, C. Teishert, F. Schmied, L. Major, B. Major. 2010. *Bulletin of the Polish Academy of Science*. 58: 2.
(10) A. S. El-Said, W. Meissl, M. C. Simon, J. R. Crespo Lopec-Urrutia, I. C. Gebeshuber, J. Laimer, H. P. Winter, J. Ullrich, F. Aumayr. 2007. Taylor & Francis. 162: 467.
(11) M. Yamagochi, Y. Yamada, J. Murase, Y. Goto, Y. Nakano, S. Hayase, M. Shikida, K. Sato. 2006. MHS2006 & Micro-Nano COE. Vol. 29.
(12) T. Aizawa, E. Iwamura, K. Itoh. 2007. *Surface & Coating Technology*. 202: 1177.
(13) E. Iwamura. 2003. Presto. 5: 166.
(14) M. Singh, Y. K Vijay, B. K. Sharma. 2007. *Pramana*. 69: 631.
(15) E. Petrova, S. Tinchev, P. Nikolova. 2011. Cornell University Library
(16) E. Asari. 2000. *Pergamon Carbon*. 38: 1857.
(17) O. Hisato, M. Yoshida, H. Yasui, K. Awazu. 2005. *Physics Research*. 242: 311.
(18) B. Iwona, J. R. Smith, A. A. Steele, I. Penegar, S. A. Campbell. 2001. *Colliods and Surfaces*. 23: 231.
(19) D. X. Ye, T. Karabacak, R. C. Picu, G. C. Wang, T. M. Lu. 2005. *Physics Publishing*. 16: 1717.